ISSN 1674-1056
http://cpb.iphy.ac.cn
http://iopscience.iop.org/cpb
中国物理 B
Chinese Physics
中国物理
Chinese Physics B

Broadband topological valley-projected edge-states transport in composite structure phononic crystal

Hong-Yong Mao(毛鸿勇), Fu-Jia Chen(陈福家), Kai Guo(郭凯), and Zhong-Yi Guo(郭忠义)

Citation: Chin. Phys. B, 2021, 30 (**8**): 084302. DOI: 10.1088/1674-1056/abea89
Journal homepage: http://cpb.iphy.ac.cn; http://iopscience.iop.org/cpb

What follows is a list of articles you may be interested in

Identifying the interactions in a colored dynamical network

Wu Zhao-Yan, Gong Xiao-Li
Chin. Phys. B, 2015, 24 (**11**): 110202. DOI: 10.1088/1674-1056/24/11/110202

Single-photon modulation spectrum

Liu Yan, Yu Bo, He Bo, Zhang Guo-Feng, Xiao Lian-Tuan, Jia Suo-Tang
Chin. Phys. B, 2014, 23 (**1**): 010101. DOI: 10.1088/1674-1056/23/1/010101

Broadband topological valley-projected edge-states transport in composite structure phononic crystal*

Hong-Yong Mao(毛鸿勇), Fu-Jia Chen(陈福家), Kai Guo(郭凯), and Zhong-Yi Guo(郭忠义)†

School of Computer and Information, Hefei University of Technology, Hefei 230009, *China*

(Received 1 December 2020; revised manuscript received 31 January 2021; accepted manuscript online 1 March 2021)

The topological valley transport, realized in phononic crystals, has aroused tremendous interest in these years. Many previous researches have further promoted the development of this transport phenomenon. Crucially, the bandwidth of the valley-projected edge mode has been an essential research topic. As is well known, the broadband will improve the adaptability of the acoustic edge-states, which will be more conducive to the transmission of information. Therefore, in this paper, we present a composite structure, composed of the atoms with different shapes forming a hexagonal lattice, which can achieve larger bandwidth than a single structure. Meanwhile, the results demonstrate that the topological protected edge states are also observed in our structure. Furthermore, the backscattering suppressions from associated valley-protected edge states under certain perturbations have also been investigated and demonstrated. Our work can provide a new idea for designing acoustic devices based on valley degree of freedom.

Keywords: valley transport, composite structures, broadband edge-states

PACS: 43.55.+p, 43.90.+v, 02.40.Pc **DOI:** 10.1088/1674-1056/abea89

1. Introduction

The discovery of quantum Hall effect (QHE)[1–4] in electronic system opens the door to the field of topological phases of matter. Since there are many similarities (in both mathematics and physics) between photonics, acoustics and the wave properties of electrons, researchers have recently created photonic and acoustic analogs with QHE. On the one hand, the first photonic mimic of quantum Hall topological insulators was achieved using a gyromagnetic material in the microwave, in which the strong magnetic field broke the time reversal symmetry (TRS).[5] On the other hand, different designing methods were proposed to implement two-dimensional acoustic topological insulators. In these systems, rotating rotors[6,7] or circulating fluids[8–11] were embedded in a supported acoustic or elastic waveguide to break the TRS. Subsequently, another way without breaking TRS, has also been proposed with the analog of quantum spin Hall effect[12–18] by constructing acoustic pesudospins.

Recently, researchers have begun to explore acoustic topological waveguides by using the acoustic analog of the quantum valley Hall effect (QVHE), which is called the acoustic valley Hall effect (AVHE).[19–28] Here, the pseudospin, labeling quantum states of energy extrema in momentum space, have been proposed.[29–33] The basic mechanism of QVHE and AVHE only need to break the space-inversion symmetry (SIS), which is relatively easy to implement in the lattice that contains Dirac dispersion at the high-symmetry points of Brillouin zone (BZ). When the SIS is broken, a band gap will be opened at the Dirac point, which will create the existing conditions for the topological edge states. In previous related work, it is generally based on the point group symmetry of C_{3V},[20,34,35] or C_{6V},[36] so that the K point of the Brillouin zone also has such a symmetry. Then by changing the radius, height, or direction of rotation of the scatterer, the symmetry will be reduced to C_3. Therefore, the Dirac cone is lifted, forming a band gap. Owing to the similarity of wave behavior in the periodic structure, the valleys also appear in artificial crystals,[19,20] in which the coupling strength and lattice symmetry between artificial atoms can be artificially regulated. At the meantime, they have a robust one-way edge state that is unaffected by the backscattering of local defects or disturbances, which can also be verified by macroscopic experimental phenomena.

Here, we propose a composite two-dimensional phononic crystals (PCs) arranged in a hexagonal lattice, which are composed of air atoms with different shapes, including circles, equilateral triangles. By comparing the band gap formed by a single structure composed of only circular air holes with that formed by a composite structure composed of circles and equilateral triangles, we confirm that the band gap formed by a composite structure with equilateral triangles has greater advantages than the above-mentioned structures. As is well known, the wider the band gap, the larger the frequency range covered by the edge states will be. Therefore, in order to efficiently control the edge states at the boundary, what we need to do is to investigate how to increase the relative width of the bulk band gap. In addition, we have also achieved topologically protected edge states by strongly suppressing the

*Project supported by the National Natural Science Foundation of China (Grant No. 61775050) and the Fundamental Research Funds for the Central Universities, China (Grant No. PA2019GDZC0098).

†Corresponding author. E-mail: guozhongyi@hfut.edu.cn

© 2021 Chinese Physical Society and IOP Publishing Ltd

backscattering in the designed composite structure. The proposed method provides diverse approaches to simulating the QVHE, which has profound significance for acoustic physics researches and versatile potential applications.

2. Theory and design

Drawing the inspiration from the previous work,[37] compared with other proposed geometries, with the same strength of the symmetry-breaking perturbation, the triangular holes have the advantage of larger band gap at the K point.[38] As shown in Fig. 1(a), we first choose and use representative composite structure (circles, equilateral triangles) for forming the hexagonal lattices which are connected by gaps. In Fig. 1(a), $a = 40\sqrt{3}$ mm is the lattice constant, d is the side length of triangular air atom, r is the radius of the circular air atom, and $b = 2\sqrt{3}$ mm is the width of gaps (the distance between the blue dashed lines). In the present scenario as depicted in Fig. 1(a), any acoustic rigid material can be used in unit cell, the velocity and mass density of air are $c_0 = 343$ m·s^{-1} and $p_0 = 1.21$ kg·m^{-3}. Figure 1(b) shows the band structure of the hexagonal lattices of air atoms with different shapes, which are obtained through home-made software based on the finite-element analysis. The Floquet periodicity is used as the boundary condition for the selected unit cell as shown in Fig. 1(a). In a hexagonal lattice with C_3 symmetry, when air atoms with different shapes have the same duty ratio, meaning that they have the same area, and the Dirac point occurs at the high symmetry point K (K') of the first Brillouin zone (BZ). Then by changing the area of the circles, the degeneracy of the K point in the BZ will be opened, to form a band gap. To keep the area of the equilateral triangles and circles the same, we can choose $d = 43.1$ mm, $r = 16$ mm, and the calculation along the boundary of the irreducible BZ. We obtain the degenerate point at K as shown by the blue dashed line in Fig. 1(b). Under C_3 symmetry, the degeneracy formed by adjusting structural parameters is called accidental degeneracy.[39] In order to effectively generate broadband, meaning that the area difference S between the circle and the equilateral triangle is large enough. For example, when $d = 43.1$ mm and $r = 21.14$ mm ($\Delta S = 500$ mm^2) as depicted by the solid red line in Fig. 1(b), the degenerate point will be broken to form two energy extreme points K_1 and K_2, which are called the acoustic valley separated by broadband gap spanning from 2075.9 Hz to 2580 Hz, and the relative bandwidth reaches 22%. In the momentum space, the distance between the two unequal energy valleys is far enough to suppress the inter-valley scattering,[31,40,41] which makes the valley a good index describing the topological state.

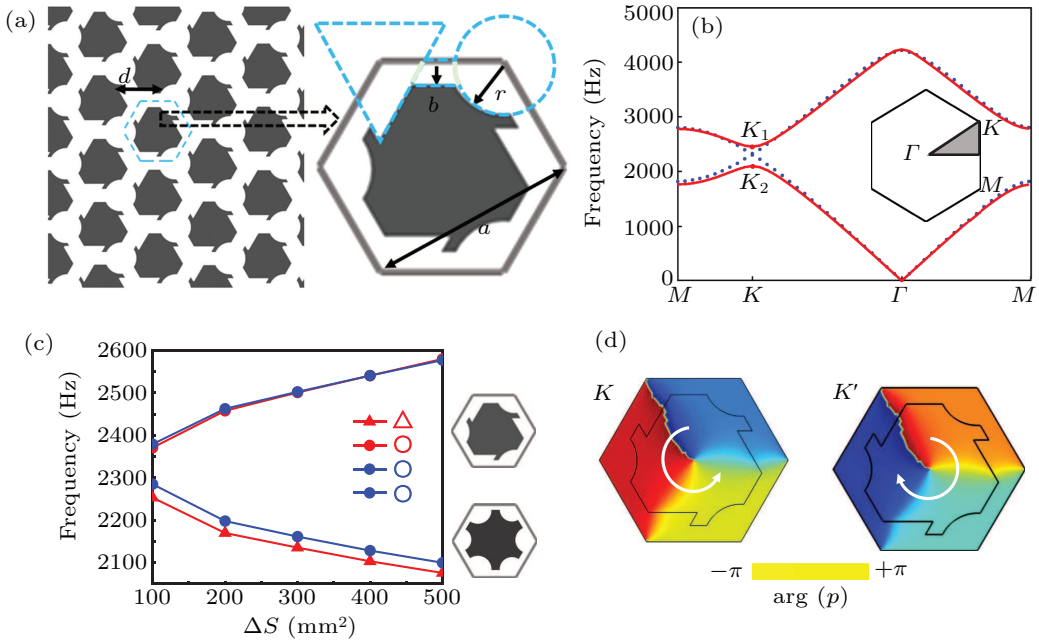


Fig. 1. (a) Overlooking schematic view of the unit cell, where b is the width of the gaps (the distance between the blue dashed lines), r is the radius of the circle, d is the side length of the equilateral triangle, and a is the lattice constant. The blue dashed triangle and circle completely show the composition of the phononic crystal cell. (b) Band diagram when the circles and triangles have the same duty ratios, namely they have the same area, the blue dashed line degenerates at the high symmetric point K or K'. When the degenerate point is lifted, like the solid red line, forming two valleys K_1 and K_2. The illustration is the first Brillouin zone of the structure. (c) Change of bandwidth with ΔS ($\Delta S = S_1 - S_2$) of the two combined structures, where S_1 is the area of circular and S_2 is the area of triangular. The red mark is a compound structure composed of equilateral triangles and circles, the blue mark is a single structure composed of circles. On the right is the structure corresponding to the two curves. (d) Pressure phase distributions at points K and K' at a frequency of 2301.8 Hz.

Then, by adjusting the area through increasing radius, the area difference ΔS can be obtained, from which the controllable band gap can be obtained as depicted in Fig. 1(c). There are two combinations in Fig. 1(c), where red line represents a composite PC structure composed of equilateral triangles and circles (the unit cell is shown in the illustration on

the right in Fig. 1(c)), and blue line is a single PC structure composed of circles with different areas. We can see that at 100 mm^2 $< \Delta S <$ 500 mm^2, the frequency difference formed by up and down frequency gradually increases in the red curve, and meanwhile, at the same ΔS, the bandwidth of the red line is obviously larger than that of the blue line, which indicate that the band gap formed by the composite structure will be wider than the single structure. As a comparison, this superior result can be attributed to the symmetrical characteristics of the triangle. That is, distributions with different shapes lead to different coupling strength between adjacent sites, and the triangle structure is an optimal result. This design concept is clearly different from the scheme of increased bandwidth proposed by some previous researchers.[42,43]

Meanwhile, we also obtain pressure phase distributions at frequency extreme points, the corners of the first Brillouin zone: K and K' points. These two asymmetrical K points are time-reversed. Therefore, the eigenstates of two K points should have different field distributions. As shown in Fig. 1(d), the left panel is the vortex field at K point (counterclockwise), and the right part is that in K' point (clockwise) at a frequency of 2301.8 Hz.

3. Results and discussion

When the PCs have slight inversion symmetry broken, acoustic valley Hall (AVH) phase transitions can be revealed by $\boldsymbol{k}\cdot\boldsymbol{p}$ perturbation method.[20] To describe the dispersion relationship in the k-valley, the effective Hamiltonian[29,37] of the k-valley can be expressed as

$$H = v_{\mathrm{D}}\left(\delta k_x \sigma_x + \delta k_y \sigma_y\right) + m v_{\mathrm{D}}^2 \sigma_Z, \tag{1}$$

$$\delta\boldsymbol{k} = \left(\delta k_x, \delta k_y\right) = \boldsymbol{k} - \boldsymbol{k}_K, \tag{2}$$

where v_{D} represents the group velocity of the K point degenerate state, $\delta\boldsymbol{k}$ is the distance of wave vector k from point k, $\sigma_{i(i=x,y,z)}$ is the Pauli matrices, and m is the effective mass defined as $m = (\omega_{\boldsymbol{q}+} - \omega_{\boldsymbol{p}-})/(2V_{\mathrm{D}}^2)$, and it is proportional to the interval between frequencies of the $\psi_{\boldsymbol{q}+}$ state and the $\psi_{\boldsymbol{p}-}$ state. The Berry curvature of the valley-dependence can be written as[29,44]

$$\Omega_{K(K')}\left(\delta\left(k\right)\right) = \frac{m v_{\mathrm{D}}}{2\left(\delta k^2 + m^2 v_{\mathrm{D}}^2\right)^{3/2}}. \tag{3}$$

Like in the electronic system, the Chern number can also be used in the acoustic system to define the PCs' valley topological properties. The number of quantized valleys can be obtained by integrating the Berry curvature over the whole BZ. The valley Chern numbers are given by

$$C_{K(K')} = \frac{\int \Omega_{K(K')}\left(\delta k\right) \mathrm{d}S}{2\pi} = \frac{1}{2}\mathrm{sgn}\left(m\right). \tag{4}$$

In the same type of the PC, the unequal energy valleys have equal numbers but the opposite signs. The topological index in the K (K') is 1/2 ($-1/2$), denoted by "+" ("–") sign as illustrated in Fig. 2(a). Therefore, the valley Chern number is equal to $+1$ or -1 ($C = C_K - C_{K'}$), indicating that due to the bulk-edge correspondence[45,46] the topological edge modes should be expected at the interface between the domains of two different topological numbers.

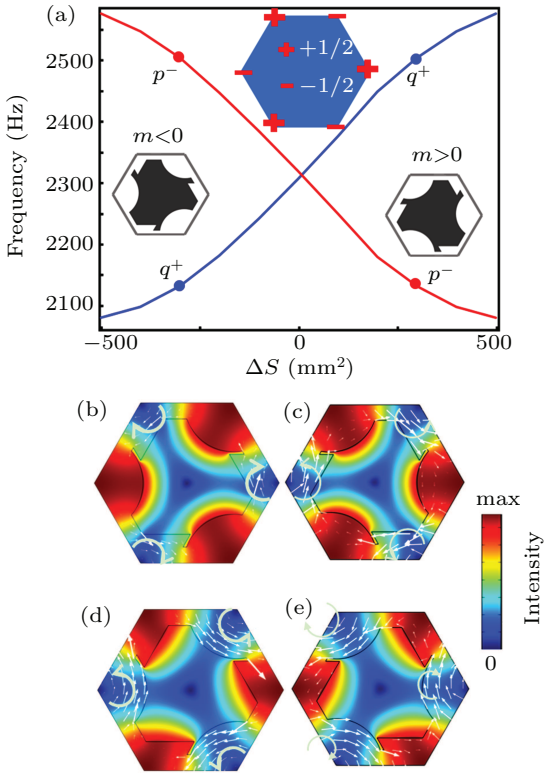


Fig. 2. (a) Evolutions of eigenmodes with ΔS. On the left side of the intersection ($\Delta S < 0$), the area of the circle is larger than the area of the triangle, on the right side, the circle and triangle exchange their sites ($\Delta S > 0$). The illustration represents different topological indices at K (K'). Panels (b)–(e) correspond to the sound field distributions of $q+$ and $p-$, respectively.

The eigenfrequency in the k as a function of ΔS is shown in Fig. 2(a). The topological phase transition process is realized by exchanging the triangle and circle positions under the same ΔS. That is, when $\Delta S > 0$, the circle is placed at the original triangle position, and the structural evolution is illustrated in Fig. 2(a). The results show that when ΔS changes from negative to positive value, the two states cross with each other, and the degenerate point occurs at $\Delta S = 0$. It can also be seen from Fig. 2(a) that there seem to be no changes for the band gaps on the left side and right side of the intersection point, but the band is reversed. We use $q+$ and $p-$ to represent the clockwise and counterclockwise energy flows in the eigenmodes. At $\Delta S < 0$, the open valley states are marked with $q+$ and $p-$, in which $\omega_{\boldsymbol{q}+} < \omega_{\boldsymbol{p}-}$, and the effective mass m is negative ($m < 0$). At $\Delta S > 0$, $\omega_{\boldsymbol{q}+} > \omega_{\boldsymbol{p}-}$, and the effective mass m is positive ($m > 0$). Such a phenomenon can be observed in Figs. 2(b)–2(e). They correspond to the points in

Fig. 2(a), respectively. We can conclude that the band inversion of the acoustic valley states can be used to characterize the AVH phase transition. The direction of the energy flow is indicated by the white arrow inside the unit cell, the vortex chirality of this energy flow can be referred to as pseudospin.[47,48] The rainbow color represents the intensities of the pressure of the four eigenmodes.

Topologically protected edge modes on the interface can be also calculated in supercell models. Therefore, we design a strip supercell structure consisting of 20 unit cells, each consisting of domain A and domain B ($\Delta S = \pm 500$ mm^2). A (referred to as domain A) and B (referred to as domain B) are the PCs with two different parameter configurations, respectively. The band structure of the A-type and B-type PCs are the same but belong to different topological phases. It should be noted that the constructed domains still retain the hexagonal structure of the atom, otherwise the edge states will not emerge in later studies. The difference between the two types of the PCs lies in a non-zero valley Chern number, which means that there is a topological phase transition from one system to another. In order to achieve the dispersion properties of waveguide composed of a composite structure, in the simulation, the periodic boundary conditions are imposed in the x axis direction along the supercell before calculating the eigenvalues and the supercell has a finite size along the y axis. In order to fully display the details of the upper part and lower part of the unit cell in the striped supercell as shown Fig. 3(a), we calculate the results of two-period structures. The topological edge state (solid red line) appears clearly in the valley K (K') between the two domains, in which the blue domain is the overlapped bulk energy band of two phononic crystals. Owing to the decrease of symmetry at the interface, there is a small band gap between the edge state and the below bulk. At the same time, we calculate the pressure filed along the blue dashed line on the y axis in Fig. 3(a), in which the energy is concentrated at the interface between the supercell A and supercell B, and it decreases exponentially inward to the bluk, as shown by the cyan curve in Fig. 3(b).

Based on the above analysis, by carefully designing the parameters of the composite structure, the edge states can be obtained at interfaces with an opposite valley Chern number. Subsequently, different kinds of defects are introduced into our topological waveguide structure to study the robustness of the topological edge states. Two types of representative defects (*i.e.*, cavity on the linear interface and at Z-shaped interface) are constructed in Figs. 4(a) and 4(d). The interfaces of waveguide are shown in the red dashed line. In the simulation, the edge states are excited by source (blue pentagram) located at the left entrance of two boundaries. Figures 4(b) and 4(c) show the topologically protected edge states, which are unidirectionally transmitted in a linear waveguide at 2400 Hz and smoothly pass through the cavity with defects (The cavity is made by removing a structure as illustrated in Fig. 4(c)). It is found that the sound waves travel unimpeded along the boundary, with no reflection appearing, just as they travel along a straight boundary. We then also analyze another defect as shown in Figs. 4(d) and 4(e), and the Z-shaped superlattice is composed of supercell A and supercell B with a 120°-sharp bend. As shown in Fig. 4(e), the sound energy is concentrated at the interface and has a uniform amplitude, indicating no strong scattering at the sharp bends. Furthermore, we also calculate the transmission spectra of these three waveguides separately, as shown in Fig. 4(f). The edge state covers the entire shadow area. Owing to the robust characteristics of the edge state protected by the topology under certain perturbations,[49] the waveguide still exhibits strong transmittance even with the introduction of a cavity and sharp bends into the interface. And as the different precisions are set in the simulation, there are differences between waveguides.

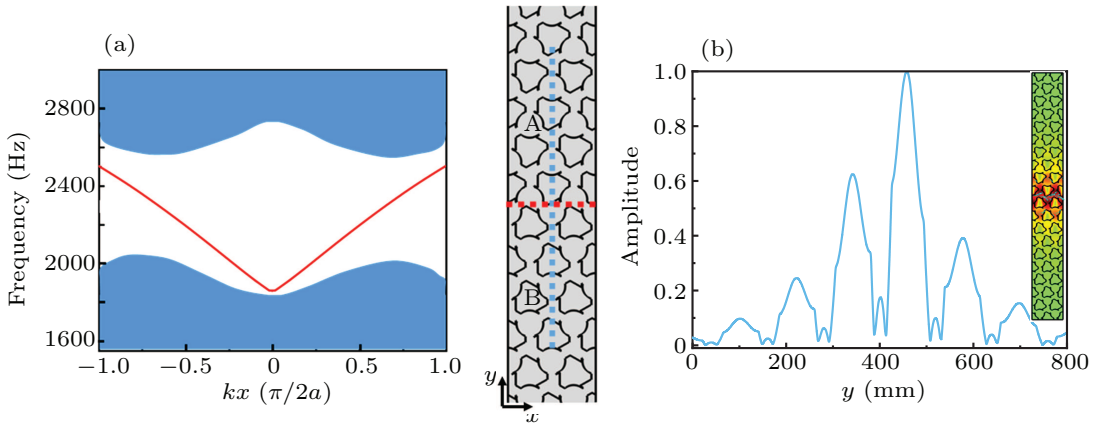


Fig. 3. (a) Calculated band structure of supercell comprising a phononic crystal. The phononic crystal interface (the red dashed line) along the x direction refers to the A–B superlattice structure (domain A: ten unit cells; domain B: ten unit cells). The red solid line is the edge state in the band gap, and the blue area of the upper part and lower part each are in a bulk state. (b) Amplitude of sound pressure field and local field intensity of edge state.

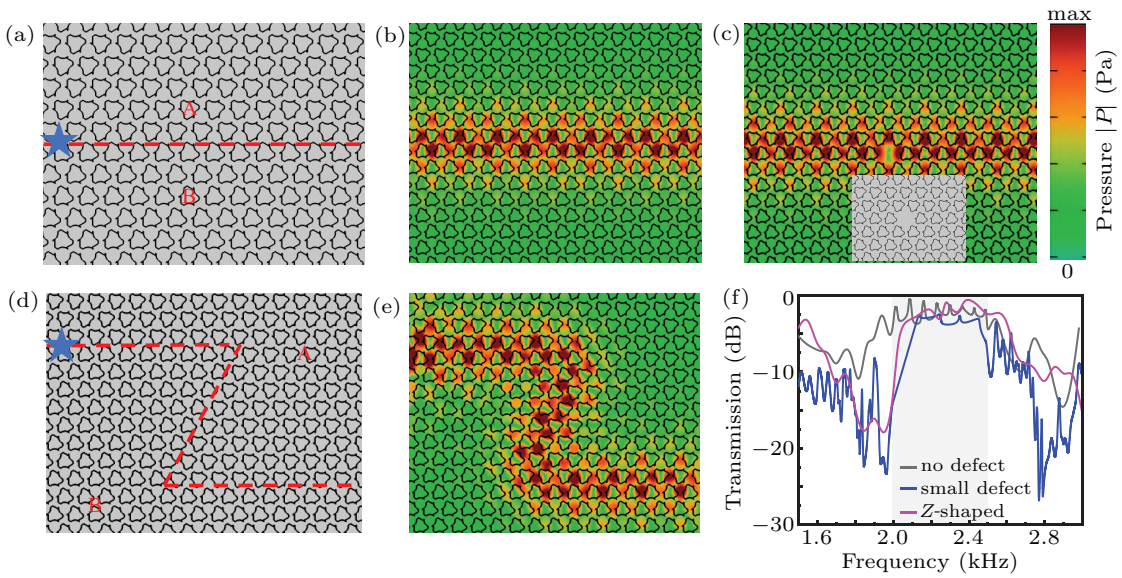


Fig. 4. (a) Straight waveguide with different interfaces (red dashed line) consisting of A (upper panel) and B (lower panel). The blue pentagram represents the location of the sound source. (b) Distribution of sound pressure field in straight waveguide. (c) Straight interface inserted with a small cavity defect, with inset showing local structure of the defect illustratively. (d) *Z*-shaped waveguide with a sharp bend of 120°. (e) *Z*-shaped distribution of sound pressure field with 120° bending. (f) Transmission spectra along three waveguides: straight waveguide (black), small defect (blue), *Z*-shaped (magenta). The shadow region (2.0 kHz–2.5 kHz) represents the bandgap of the edge state for three-type waveguides.

4. Conclusions

In this work, we present the design of a composite phononic crystal to realize the valley as the analogue of the QVHE. By adjusting the sites of different shapes, we obtain the AVH phase transition characterized by the inversion of valley Chern number. More importantly, compared with the same type of structure, the mixed type of atoms with equilateral triangle designed by us can bring about larger bandwidth undoubtedly. The increase of bandgap width improves the adaptability of topological edge states. Simultaneously, the valley-projected topological edge-states that suppresses backscattering can be found on a domain wall that separates different areas with opposite valley Chern numbers. In addition, the chiral characteristics of the valley provide a new way for people to manipulate sound waves and enrich the physical connotation of sound waves lacking spin freedom. Our results provide an idea for designing acoustical devices based on AVHE.

References

[1] Klitzing K, Dorda G and Pepper M 1980 *Phys. Rev. Lett.* **45** 494
[2] Thouless D J, Kohmoto M, Nightingale M P and Nijs M den 1982 *Phys. Rev. Lett.* **49** 405
[3] Arbab A I 2013 *Chin. Phys. B* **21** 127301
[4] Tarkhanyan R H and Uzunoglu N K 2000 *PIER* **29** 321
[5] Wang Z, Chong Y, Joannopoulos J D and Soljačić M 2009 *Nature* **461** 772
[6] Wang P, Lu L and Katia Bertoldi 2015 *Phys. Rev. Lett.* **115** 104302
[7] Nasha L M, Klecknera D, Reada A, Vitellib V, Turnerc A M and Irvine W T M 2015 *Proc. Natl. Acad. Sci. USA* **112** 14495
[8] Yang Z J, Gao F, Shi X H, Lin X, Gao Z, Chong Y D and Zhang B L 2015 *Phys. Rev. Lett.* **114** 114301
[9] Khanikaev A B, Fleury R, Mousavi S H and Alu A 2015 *Nat. Commun.* **6** 8260
[10] Chen Z G and Wu Y 2016 *Phys. Rev. Appl.* **5** 054021
[11] Xu N, He C, Sun X C, Liu X P, Lu M H, Feng L and Chen Y F 2015 *New J. Phys.* **17** 053016
[12] Mousavi S H, Khanikaev A B and Wang Z 2015 *Nat. Commun.* **6** 8682
[13] Zhang Z W, Wei Q, Cheng Y, Zhang T, Wu D J and Liu X J 2017 *Phys. Rev. Lett.* **118** 084303
[14] Yu S Y, He C, Wang Z, Liu F K, Sun X C, Li Z, Lu H Z, Lu M H, Liu X P and Chen Y F 2018 *Nat. Commun.* **9** 3072
[15] Susstrunk R and Huber S D 2015 *Science* **349** 47
[16] Peng Y G, Qin C Z, Zhao D G, Shen Y X, Xu X Y, Bao M, Jia H and Zhu X F 2016 *Nat. Commun.* **7** 13368
[17] Rehman M Ur and Abid A A 2017 *Chin. Phys. B* **26** 127304
[18] He C, Ni X, Ge H, Sun X C, Chen Y B, Lu M H, Liu X P and Chen Y F 2016 *Nat. Phys.* **12** 1124
[19] Lu J Y, Qiu C Y, Ke M Z and Liu Z Y 2016 *Phys. Rev. Lett.* **116** 093901
[20] Lu J Y, Qiu C Y, Ye L P, Fan X Y, Ke M Z, Zhang F and Liu Z Y 2017 *Nat. Phys.* **13** 369
[21] Raj Kumar P and Massimo R 2017 *New J. Phys.* **19** 025001
[22] Liu T W and Fabio S 2018 *Phys. Rev. Appl.* **9** 014001
[23] Zhu H F, Liu T W and Fabio S 2018 *Phys. Rev. B* **97** 174301
[24] Yang Y H, Yang Z J and Zhang B L 2018 *J. Appl. Phys.* **123** 091713
[25] Nassar H, Yousefzadeh B, Fleury R, Ruzzene M, Alù A, Daraio C, Norris A N, Huang G L and Haberman M R 2020 *Nat. Rev. Mater.* **5** 667
[26] Huo S Y, Chen J J, Huang H B and Huang G L 2017 *Sci. Rep.* **7** 10335
[27] Javier Vila, Raj K Pal and Massimo Ruzzene 2017 *Phys. Rev. B* **96** 134307
[28] Li Y, Liu Y N and Zhang X 2020 *Chin. Phys. B* **29** 106301
[29] Xiao D, Yao W and Niu Q 2007 *Phys. Rev. Lett.* **99** 236809
[30] Yao W, Xu X D and Heinz T F 2014 *Nat. Phys.* **10** 343
[31] Ju L, Shi Z, Nair N, Lv Y, Jin C, Velasco J Jr, Ojeda-Aristizabal C, Bechtel H, Martin M C, Zettl A, Analytis J and Wang F 2015 *Nature* **520** 650
[32] Zhang F, MacDonald A H and Mele E J 2013 *Proc. Natl. Acad. Sci. USA* **110** 10546
[33] Li J, Wang K, McFaul K J, Zern Z, Ren Y, Watanabe K, Taniguchi T, Qiao Z and Zhu J 2016 *Nat. Nanotechnol.* **11** 1060
[34] Shen Y Y, Qiu C Y, Cai X X, Ye L P, Lu J Y, Ke M Z and Liu Z Y 2019 *Appl. Phys. Lett.* **114** 023501
[35] Geng Z G, Peng Y G, Shen Y X, Zhao D G and Zhu X F 2018 *Appl. Phys. Lett.* **113** 033503
[36] Wang Z, Liu F K, Yu S Y, Yan S L, Lu M H, Jing Y and Chen Y F 2019 *J. Appl. Phys.* **125** 044502

[37] Mikhail I S, Wiktor W, Alexander T, Xu Y and Natalia M L 2019 *Nat. Nanotechnol.* **14** 31
[38] Barik S, Miyake H, DeGottardi W, Waks E and Hafezi M 2016 *New J. Phys.* **18** 113013
[39] Lu J Y, Qiu C Y, Xu S J, Ye Y T, Ke M Z and Liu Z Y 2014 *Phys. Rev. B* **89** 134302
[40] Gorbachev R V, Song J C W, Yu G L, Kretinin A V, Withers F, Cao Y, Mishchenko A, Grigorieva I V, Novoselov K S, Levitov L S, and Geim A K 2014 *Science* **346** 448
[41] Yao W, Yang S A and Niu Q 2009 *Phys. Rev. Lett.* **102** 096801
[42] Zhang Z W, Tian Y, Cheng Y, Wei Q, Liu X J and Johan C 2018 *Phys. Rev. Appl.* **9** 034032
[43] Xia B Z, Liu T T, Huang G L, Dai H Q, Jiao J R, Zang X G, Yu D J, Zheng S J and Liu J 2017 *Phys. Rev. B* **96** 094106
[44] Zhang F, Jung J, Fiete G A, Niu Q and MacDonald A H 2011 *Phys. Rev. Lett.* **106** 156801
[45] Hasan M Z and Kane C L 2010 *Rev. Mod. Phys.* **82** 3045
[46] Kane C L and Mele E J 2005 *Phys. Rev. Lett.* **95** 146802
[47] Han X Z, Peng Y G, Li L, Hu Y J, Mei C S, Zhao D G, Zhu X F and Wang X L 2019 *Phys. Rev. Appl.* **12** 014046
[48] Yu S Y, Sun X C, Ni X, Q. Wang, Yan X J, He C, Liu X P, Feng L, Lu M H and Chen Y F 2016 *Nat. Mater.* **15** 1243
[49] Gao F, Xue H R, Yang Z J, Lai K, Yu Y, Lin X, Chong Y D, Shvets G and Zhang B L 2018 *Nat. Phys.* **14** 140